Supplementary Material:
Experimental investigation of volcaniclastic compaction during burial

Edgar U. Zorn, Jackie E. Kendrick, Anthony Lamur, Janine Birnbaum, Ulrich Kueppers, Marize Muniz da Silva, Yan Lavallée

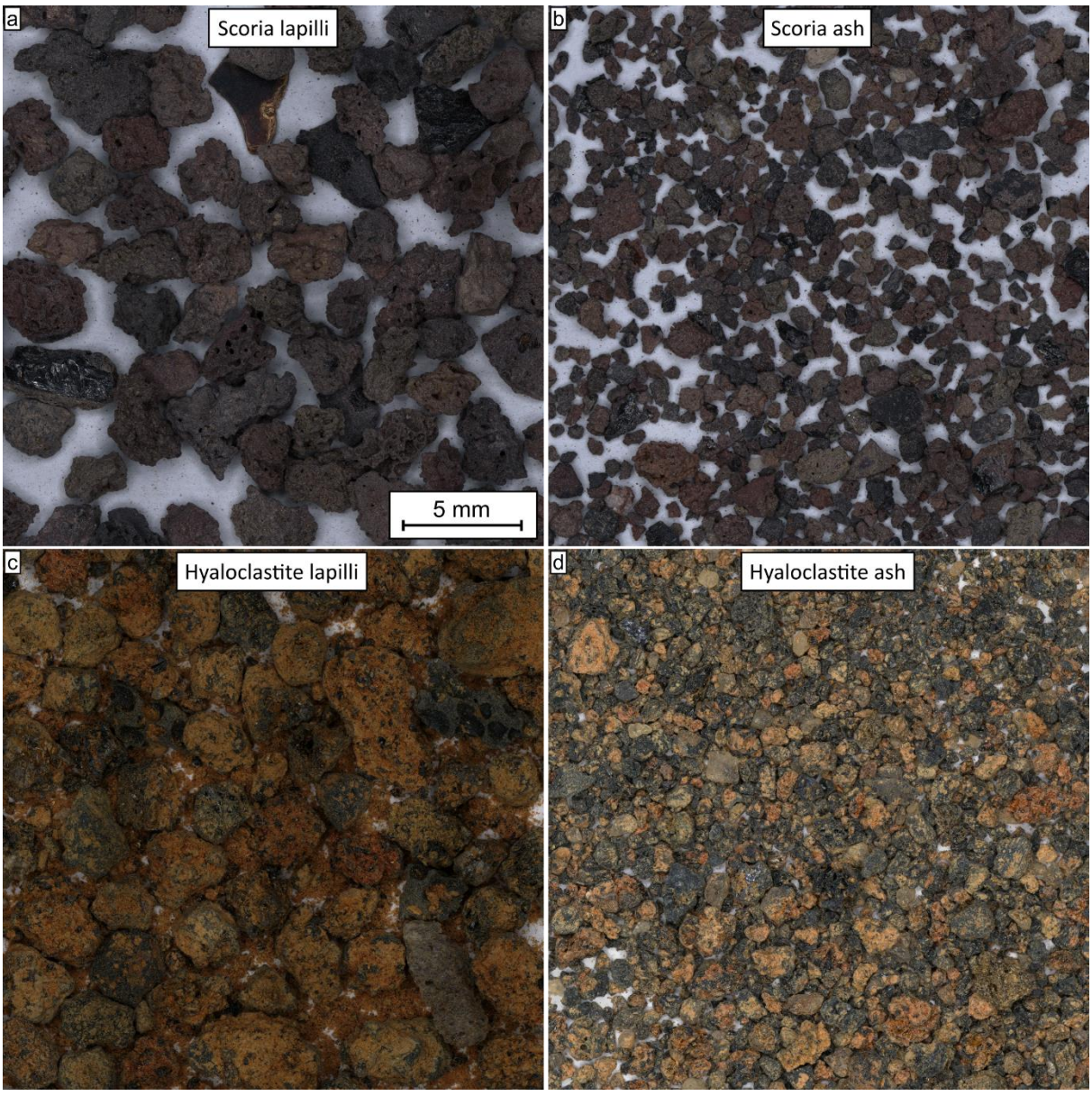

Fig. S1: Photos of the original samples sieved to lapilli and ash size fractions. (a,b) Scoria consists predominantly of porous clasts in various grey, brown and red-purple matrix colours. Phenocrysts have low abundance, but can be large, occasionally exceeding several millimetres in size. (c,d) The hyaloclastite consists of grains agglutinated dark glassy fragments coated by alteration minerals of orange, yellow and brown, which also shed as fine powder. Phenocrysts are more abundant compared to the scoria, but rarely exceed 1 mm in size.

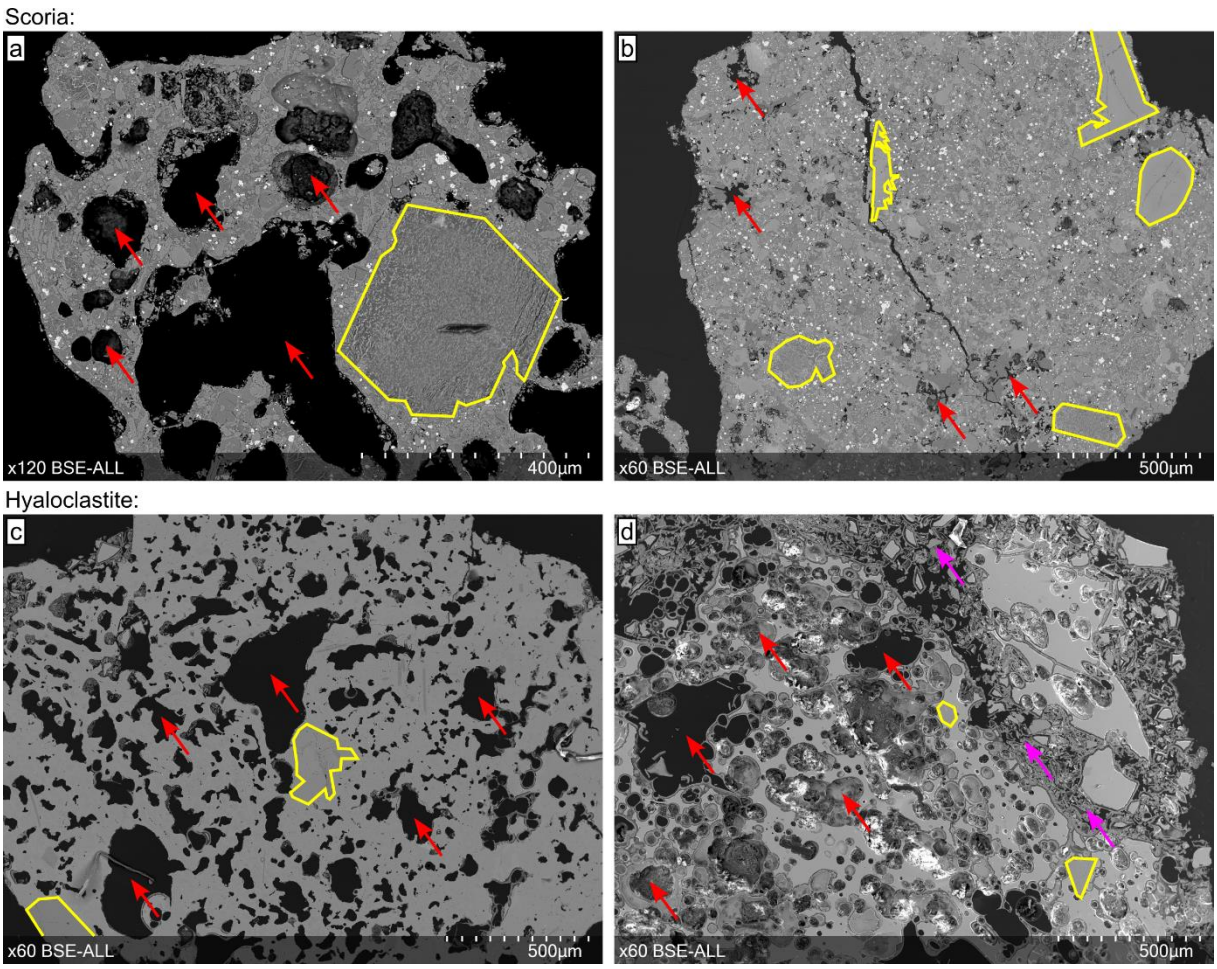

Fig. S2: Selected BSE images of the samples. (a, b) The scoria has a dominantly microcrystalline groundmass, occasional large phenocrysts (examples as yellow outlines) and highly variable grain porosities as vesicles (examples as red arrows) can be (a) large and spherical or (b) small and irregularly shaped. (c,d) The hyaloclastite comprises agglutinated glassy basalt shards of various sizes, each of which has a predominantly glassy matrix, vesicles (examples as red arrows) are smaller and more irregularly-shaped compared to the scoria, but are more homogeneously distributed and more similar grain-to-grain. Larger pores originate from sintered contacts (purple arrow) between the vesicular basalt fragments. Phenocrysts (examples as yellow outlines) are also present, but generally appear smaller than in the scoria. Various stages of alteration are depicted, from (c) almost none to (d) possessing heavily altered rims and pore-infilling mineralisation. Epoxy appears black.

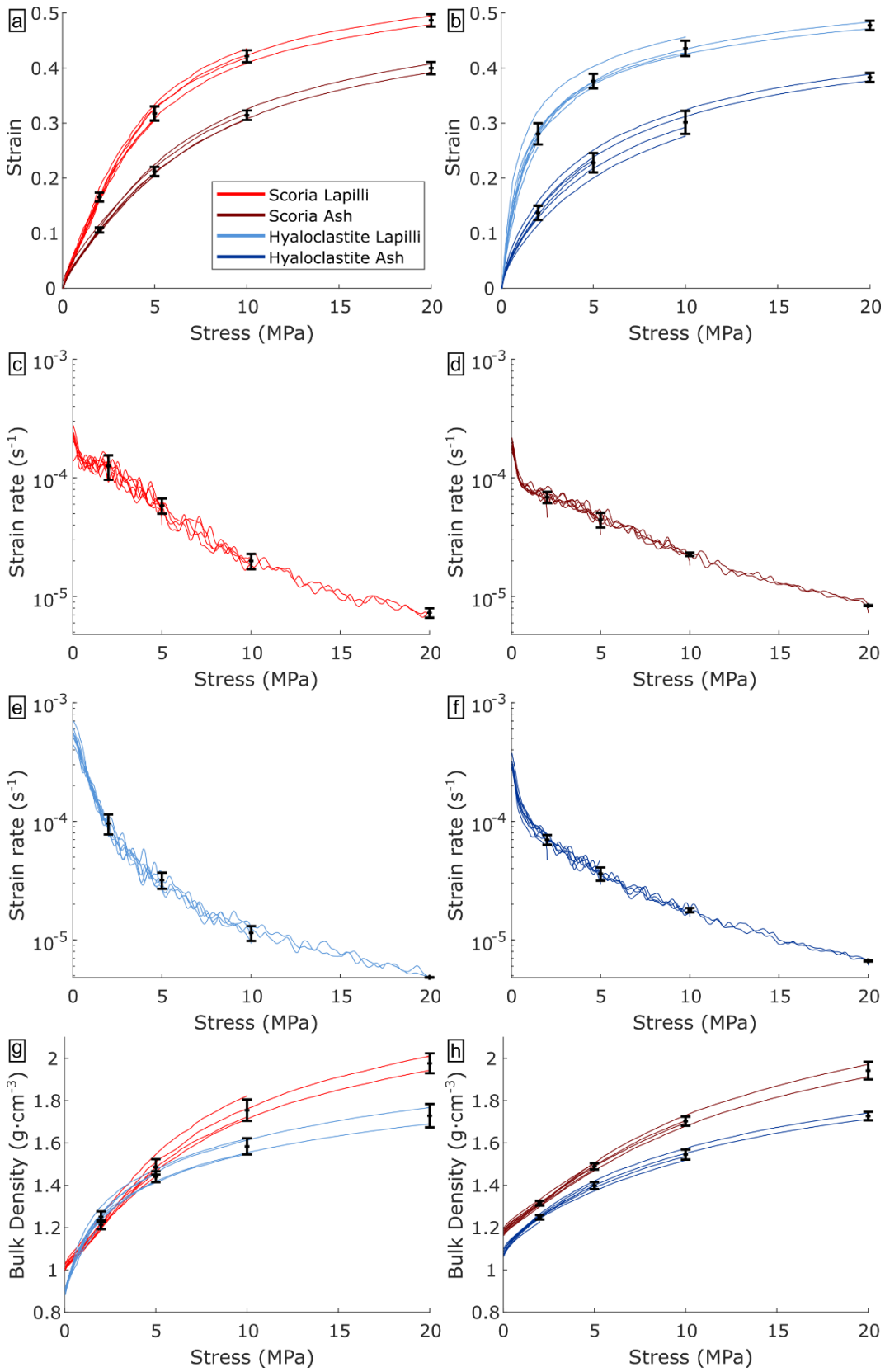

Fig. S3: Compaction curves of all experiments showing (a,b) the strain, (c-f) strain rate, and (g,h) bulk density as a function of stress. Averages and standard deviations at the target stresses are marked in black and are based on the number of experiments reaching this stress (8 at 2 MPa, 6 at 5 MPa, 4 at 10 MPa, 2 at 20 MPa). Inter-sample variability is low, however, strain and bulk density show increasing variability towards higher stresses, though the decreasing number of experiments at higher stresses also makes the repeatability assessments less reliable.

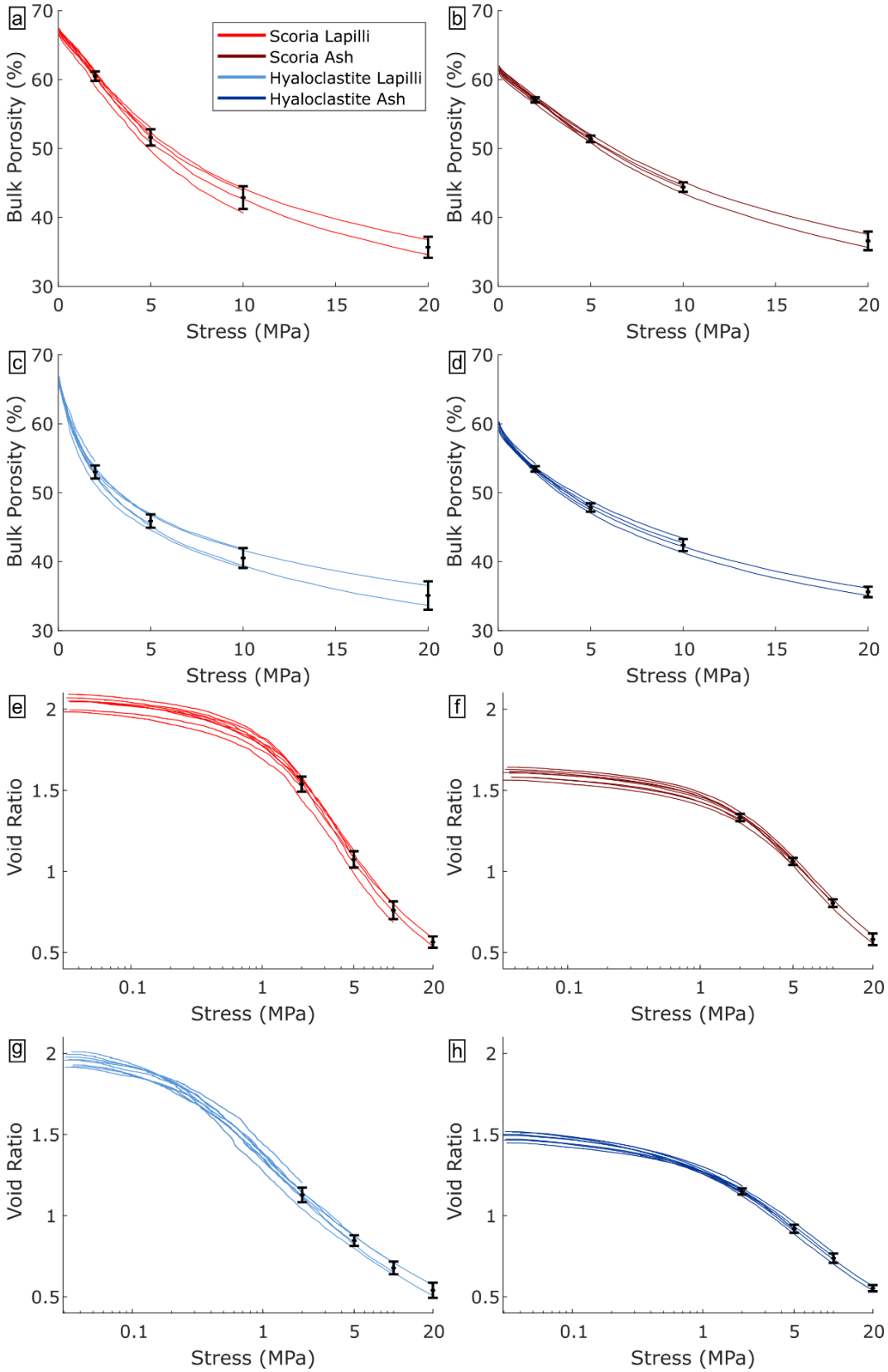

Fig. S4: Compaction curves of all experiments showing (a-d) the bulk porosity and (e-h) void ratio as a function of stress for scoria lapilli and ash, and hyaloclastite lapilli and ash. Averages and standard deviations at the target stresses are marked in black and are based on the number of experiments that reached this stress (8 at 2 MPa, 6 at 5 MPa, 4 at 10 MPa, 2 at 20 MPa).

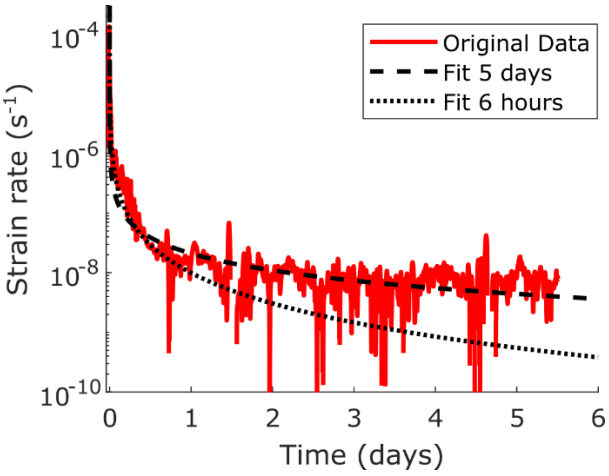

Fig. S5: Repeat experiment showing strain rates for the creep of the scoria lapilli sample at 2 MPa static stress up to ~5 days. The resulting model fit (eq. 12) is compared against the 6 hours experiment, showing a minor underestimation of long-term strain rates in the shorter experiment.

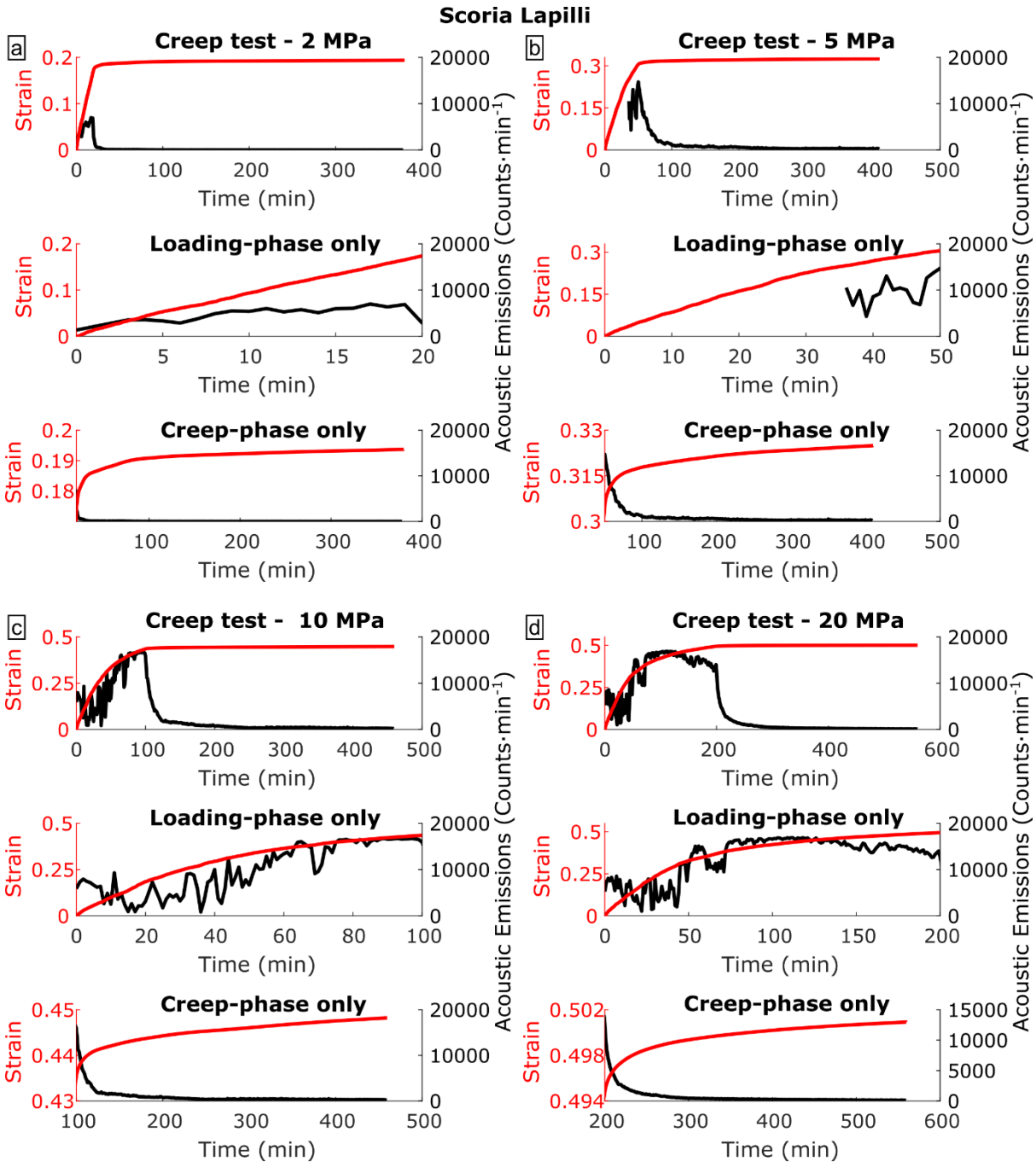

Fig. S6: All measured strains and acoustic emissions for the scoria samples in lapilli sizes during dynamic stressing (loading) and at subsequent static (creep) stresses of (a) 2 MPa, (b) 5 MPa, (c) 10 MPa and (d) 20 MPa. Each panel is split to the full experiment, then the loading and creep phases individually. The initial ~35 mins of AEs in (b) are missing due to a recording malfunction.

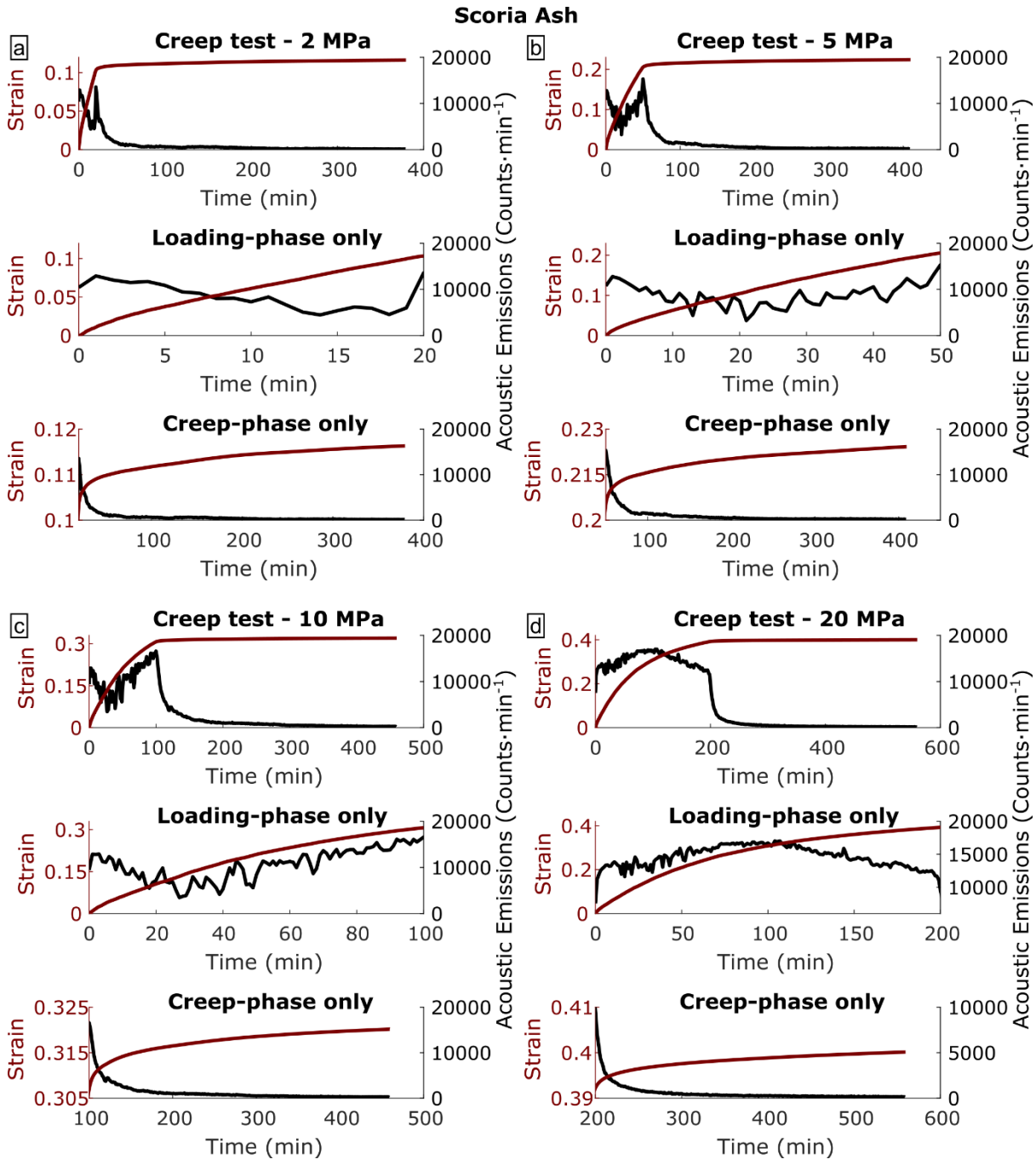

Fig. S7: All measured strains and acoustic emissions for the scoria samples in ash sizes during dynamic stressing (loading) and at subsequent static (creep) stresses of (a) 2 MPa, (b) 5 MPa, (c) 10 MPa and (d) 20 MPa. Each panel is split to the full experiment, then the loading and creep phases individually.

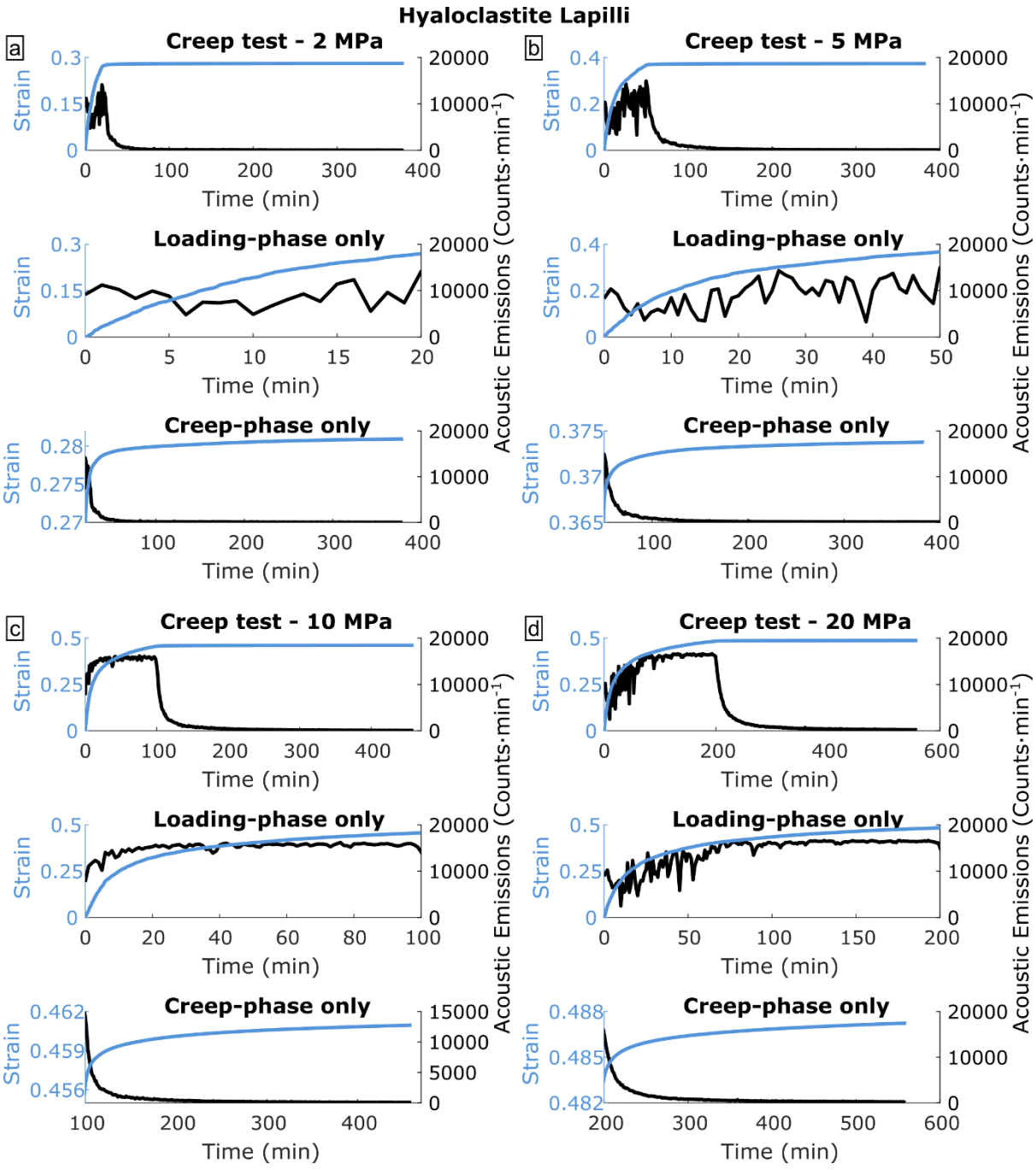

Fig. S8: All measured strains and acoustic emissions for the hyaloclastite samples in lapilli sizes during dynamic stressing (loading) and at subsequent static (creep) stresses of (a) 2 MPa, (b) 5 MPa, (c) 10 MPa and (d) 20 MPa. Each panel is split to the full experiment, then the loading and creep phases individually.

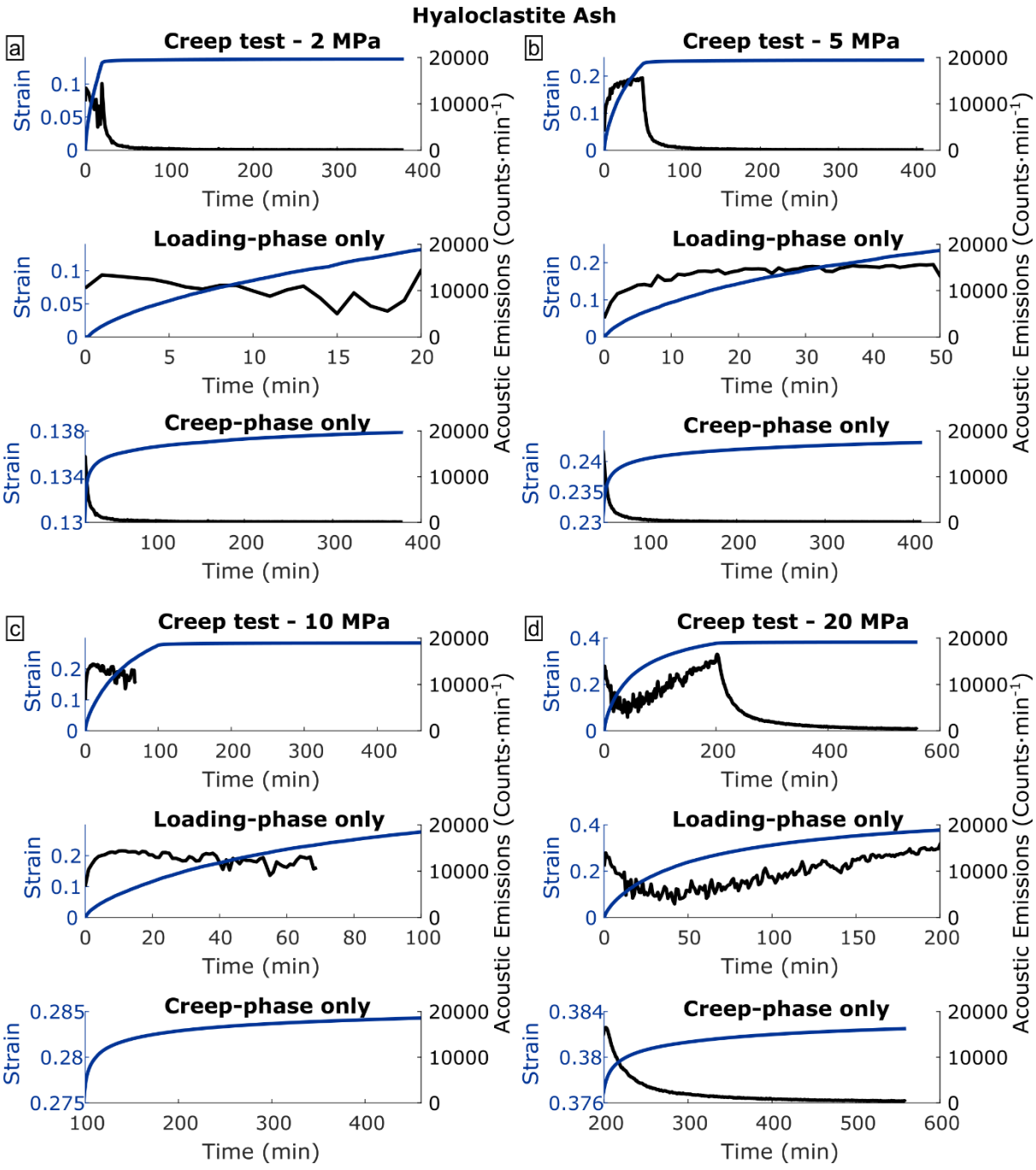

Fig. S9: All measured strains and acoustic emissions for the hyaloclastite samples in ash sizes during dynamic stressing (loading) and at subsequent static (creep) stresses of (a) 2 MPa, (b) 5 MPa, (c) 10 MPa and (d) 20 MPa. Each panel is split to the full experiment, then the loading and creep phases individually.

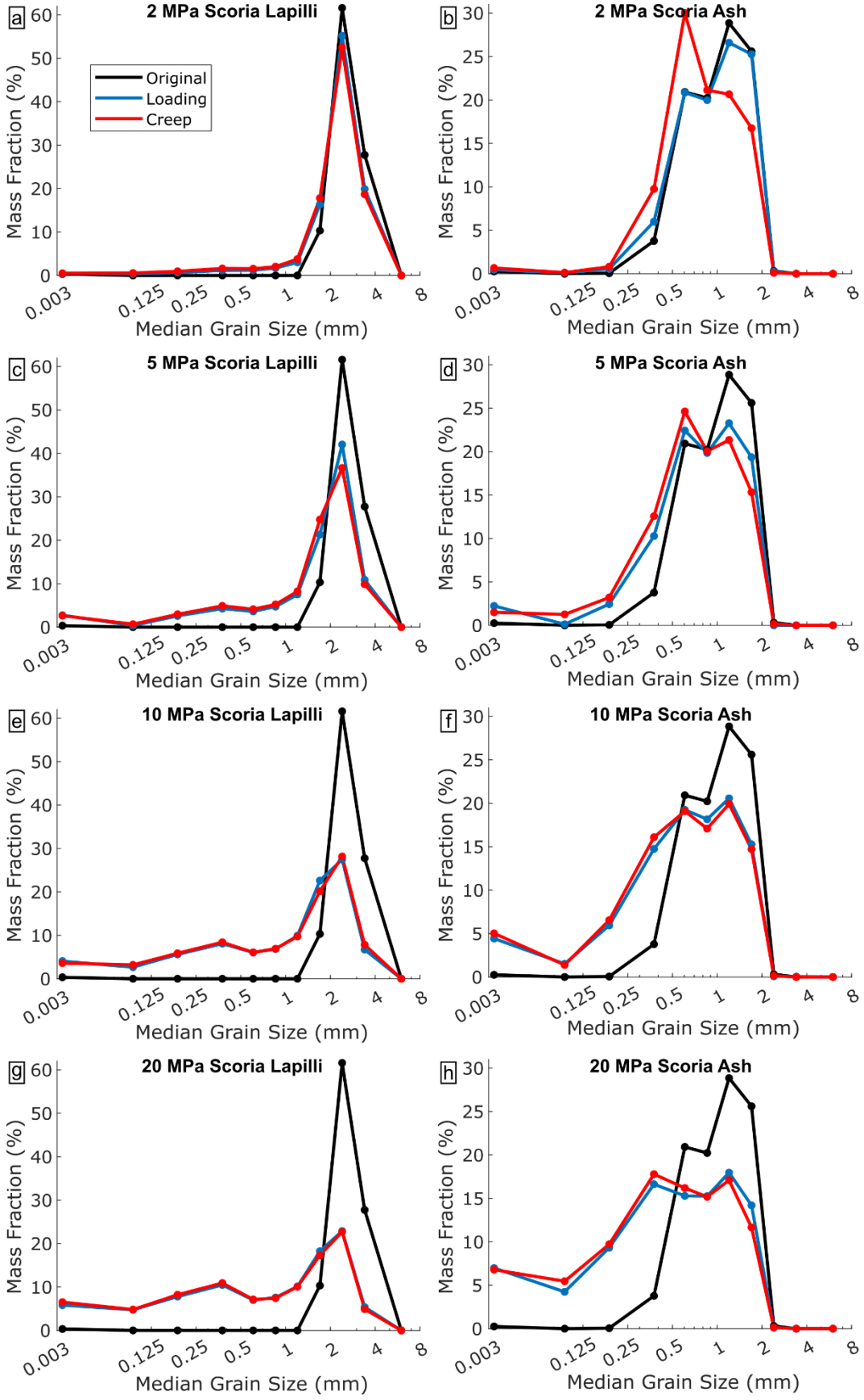

Fig. S10: Grain size comminution of the scoria after dynamic loading to the target stress (blue) and after dynamic loading plus 6 hours of creep (red) at the target static stress of (a,b) 2 MPa, (c,d) 5 MPa, (e,f) 10 MPa, and (g,h) 20 MPa for the lapilli and ash samples, respectively.

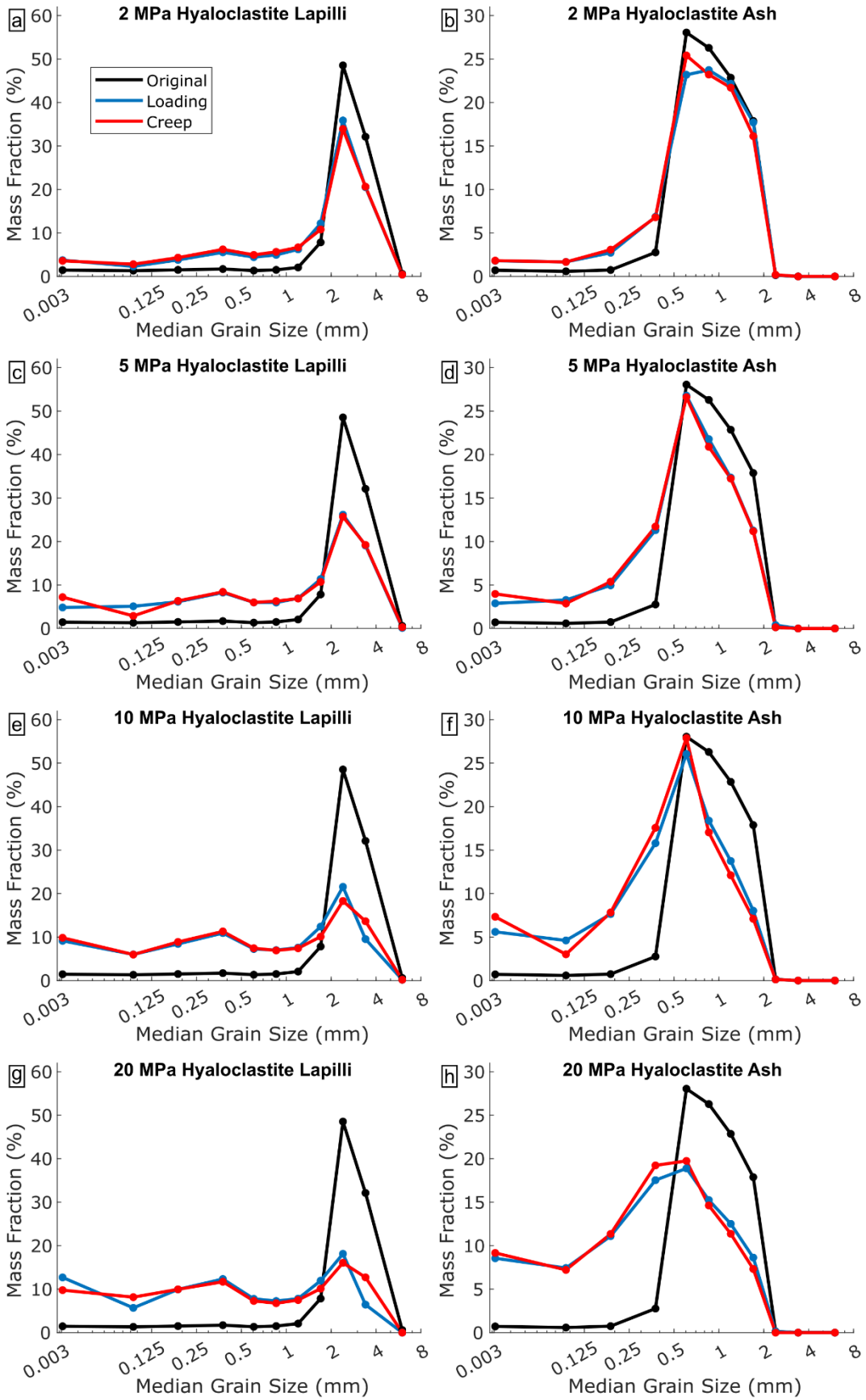

Fig. S11: Grain size comminution of the hyaloclastite after dynamic loading to the target stress (blue) and after dynamic loading plus 6 hours of creep (red) at the target static stress of (a,b) 2 MPa, (c,d) 5 MPa, (e,f) 10 MPa, and (g,h) 20 MPa for the lapilli and ash samples, respectively.

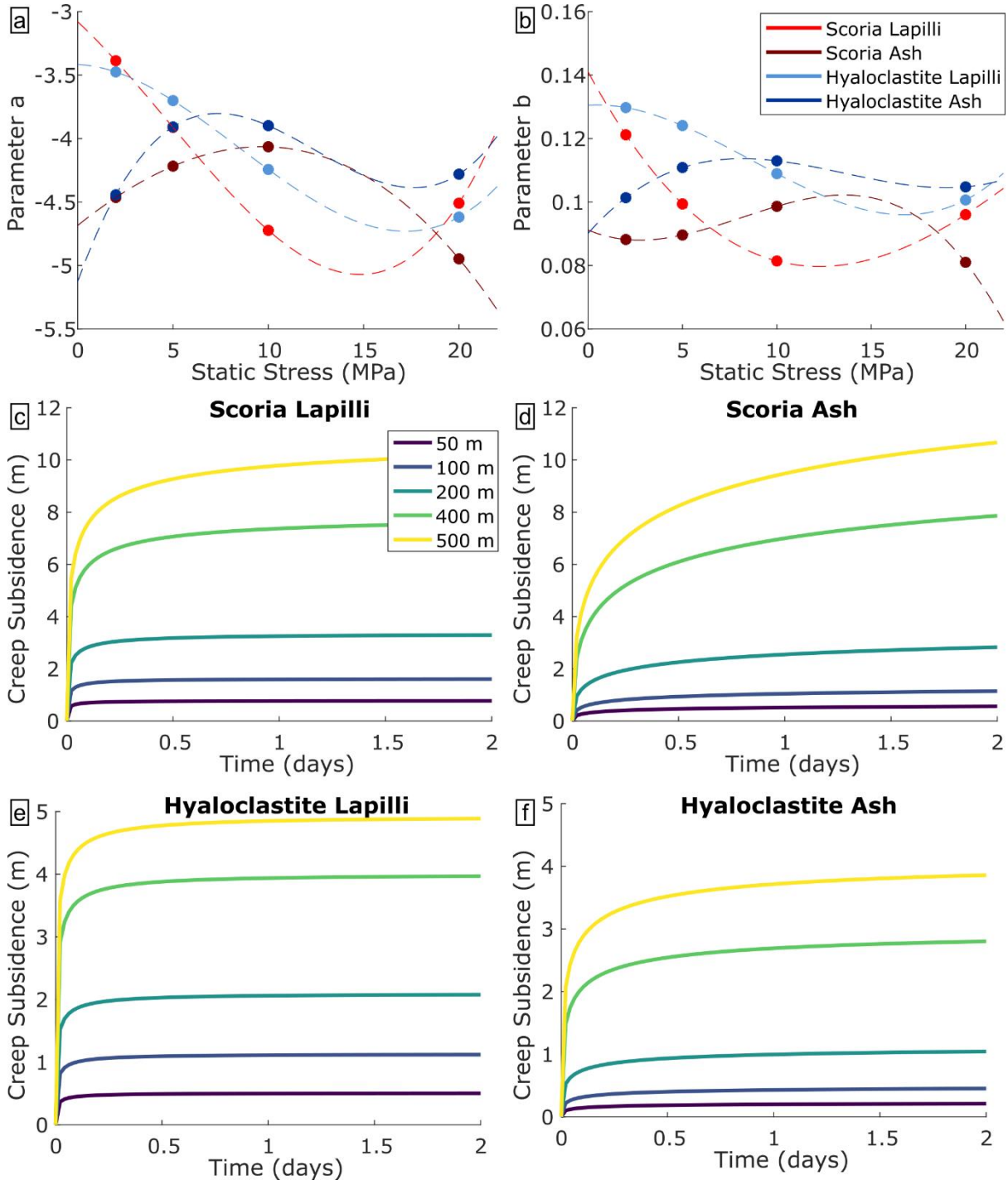

Fig. S12: Creep model data showing (a,b) the best-fitting a and b parameters see (eq. 13). The dashed lines show the spine interpolant. Model predictions for surface subsidence discretised for specific thicknesses are shown for (c) scoria lapilli, (d) scoria ash, (e) hyaloclastite lapilli, and (f) hyaloclastite ash, showing that most of the expected creep deformation occurs within the first ~2 days after deposition, then progresses much more slowly.

Supplementary Table S1: Compaction data and variability (as standard deviation) using all experiments (static and dynamic), for the dynamic portion only. The data represent the value at the point at which the sample experienced the defined stress condition. For each sample, 8 experiments reach the condition of 2 MPa, 6 reach 5 MPa, 4 reach 10 MPa and 2 reach 20 MPa (as 2 tests were stopped at each condition for physical examination). The pre-compression stress σ_P and the compression index C_c are calculated for the entire sample averages from all experiments (except 2 MPa as the stress was insufficient to determine these values).

Sample	Stress (MPa)	Strain		Porosity (%)		Density (g·cm^{-3})		Void Ratio		σ_P (Mpa)		C_c	
		AVG	STD	AVG	STD	AVG	STD	AVG	STD	AVG	STD	AVG	STD
Scoria Lapilli	2	0.1655	0.0083	60.492	0.6895	1.214	0.0212	1.5604	0.0234	0.9933	0.0933	1.1908	0.0828
	5	0.3175	0.0128	51.6058	1.1839	1.4871	0.0364	1.0951	0.0384				
	10	0.4215	0.0111	42.8815	1.6453	1.7552	0.0506	0.7748	0.0303				
	20	0.4867	0.0112	35.675	1.5266	1.9766	0.0469	0.5646	0.0346				
Scoria Ash	2	0.1056	0.0046	57.0518	0.3712	1.3156	0.0114	1.3659	0.0161	1.4150	0.0677	0.8175	0.0571
	5	0.2121	0.0084	51.3883	0.4819	1.4891	0.0148	1.0845	0.0279				
	10	0.3143	0.0087	44.4064	0.6956	1.703	0.0213	0.8118	0.0283				
	20	0.3999	0.0111	36.5995	1.3578	1.9421	0.0416	0.5815	0.0359				
Hyaloclastite Lapilli	2	0.2804	0.0192	53.0145	0.946	1.2516	0.0252	1.1280	0.0451	0.2417	0.0337	0.7720	0.0314
	5	0.3765	0.0132	45.897	0.9669	1.4412	0.0258	0.8464	0.0327				
	10	0.436	0.0139	40.5321	1.4391	1.5841	0.0383	0.6776	0.0393				
	20	0.4776	0.0086	35.0948	2.0585	1.7289	0.0548	0.5400	0.0469				
Hyaloclastite Ash	2	0.1369	0.0129	53.4497	0.3985	1.2488	0.0107	1.1492	0.0187	0.9767	0.1783	0.6115	0.0095
	5	0.2279	0.0176	47.8607	0.6166	1.3987	0.0165	0.9194	0.0249				
	10	0.3013	0.0209	42.4029	0.8687	1.5452	0.0233	0.7380	0.0289				
	20	0.3831	0.0083	35.6127	0.7583	1.7273	0.0203	0.5527	0.0194				